MDPI

Article

Fault Diagnosis of Permanent Magnet Synchronous Motor of Coal Mine Belt Conveyor Based on Digital Twin and ISSA-RF

Yourui Huang [1,2], Biao Yuan [1,*], Shanyong Xu [1] and Tao Han [1]

1   School of Electrical & Information Engineering, Anhui University of Science and Technology, Huainan 232001, China
2   School of Electrical and Opto Electronic Engineering, West Anhui University, Lu'an 237012, China
*   Correspondence: 2020200797@aust.edu.cn

Abstract: Permanent magnet synchronous motors (PMSMs) have been gradually used as the driving equipment of coal mine belt conveyors. To ensure safety and stability, it is necessary to carry out real-time and accurate fault diagnosis of PMSM. Therefore, a fault diagnosis method for PMSM based on digital twin and ISSA-RF (Improved Sparrow Search Algorithm Optimized Random Forest) is proposed. Firstly, the multi-strategy hybrid ISSA is used to solve the problems of uneven population distribution, insufficient population diversity, low convergence speed, etc. In addition, the fault diagnosis model of ISSA-RF permanent magnet synchronous motor is constructed based on the optimization of the number of Random Forest decision trees and that of features of each node by ISSA. Secondly, considering the operation mechanism and physical properties of PMSM, the relevant digital twin model is constructed and the real-time mapping of physical entity and virtual model is realized through data interactive transmission. Finally, the simulation and experimental results show that the fault diagnosis accuracy of ISSA-RF, 98.2%, is higher than those of Random Forest (RF), Sparrow Search Algorithm Optimized Random Forest (SSA-RF), BP neural network (BP) and Support Vector Machine (SVM), which verifies the feasibility and ability of the proposed method to realize fault diagnosis and 3D visual monitoring of PMSM together with the digital twin model.

Keywords: digital twin; belt conveyor; permanent magnet synchronous motor; Random Forest; sparrow search optimized algorithm; fault diagnosis

1. Introduction

The coal mine belt conveyor is very important transportation equipment in coal mining, and is advantageous in that it is effective over long transmission distances, has strong transmission capacity and works continuously [1,2]. The composition of a coal mine belt conveyor is shown in Figure 1; it mainly includes a driving motor, a belt, a transmission device, a tensioning device, a driving roller and an idler. The efficiency of coal mine transportation is directly related to the belt conveyor. Most of the traditional belt conveyors are driven by AC asynchronous motors and deceleration devices with disadvantages such as low transmission efficiency, poor speed regulation and difficulty in intelligent control [3,4]. Thus, Permanent Magnet Synchronous Motors (PMSMs) have been widely used in various fields due to their high efficiency, high torque mass ratio, stable operation and good control performance [5]. They have been increasingly used as a source to drive equipment in the process of coal mining [6–8]. The high efficiency and energy saving of belt conveyors depends on the choice of driving mode. Reference [9] pointed out that belt conveyors adopt both a permanent magnet motor and a frequency conversion driving system, which means they have greater energy-saving capacity than the previous driving systems. Feng Guihong et al. proposed a belt conveyor directly driven by an external rotor permanent magnet synchronous motor, which was advantageous in its high torque, adjustable speed and high efficiency [10]. To ensure safe and stable power

output in the process of coal mining, it is necessary to carry out daily maintenance and fault diagnosis for the power driving equipment. For the belt conveyor driven by PMSM, how to make intelligent, accurate and efficient fault diagnosis concerning the PMSM is the key direction of research. The failure of PMSM may lead to a significant decline in its performance, resulting in high losses in the process of coal mining.

(**a**)

(**b**)

Figure 1. Coal mine belt conveyor: (**a**) illustration of model; (**b**) object pictures.

Until now, many scholars have carried out in-depth research on the fault diagnosis of PMSM, and the main fault diagnosis methods generally include: diagnosis method based on model [11–13], diagnosis method based on signal processing [14,15] and diagnosis method based on artificial intelligence machine learning [16–18]. Haddad et al. established three fault models of PMSM by using finite element analysis, and judged the faults by using voltage and current characteristics of the motor [19]. Arellano-Padilla. J et al. adopted the high-frequency signal injection method to diagnose the inter-turn short circuit fault of PMSM online [20]. Alameh et al. extracted the key features of motor health and failure from the vibration signals of PMSM to realize the fault diagnosis of the motor [21]. Alvarez-Gonzalez F proposed a method for fault detection of PMSM stator windings by using the Hilbert–Huang Transform [22]. Ullah et al. used the Visual Geometry Group (VGG) network to extract the features of the stator current and vibration signals of PMSM, and converted the feature signals into images to achieve motor fault diagnosis [23]. DOĞAN Zafer et al. proposed a method based on Empirical Mode Decomposition (EMD) and statistical analysis to realize fault diagnosis of PMSM stator windings [24].

With the rapid development of big data, artificial intelligence, sensors and other technologies, coal mining is gradually shifting to informatization, digitalization and intelligence [25]. The rapid development of digital twin provides strong support for the digitalization and intelligent mining of coal mines. Digital twin was first proposed by Professor Michael Grieves in the Product Lifecycle Management course of Michigan University in 2003 [26]. It realizes the interactive mapping of the physical world and the virtual information world by establishing a digital virtual model with multi-physical, multi-scale and multi-disciplinary attributes [27]. Digital twin technology plays an important role in different fields. To sum up, this paper proposes a fault diagnosis method of PMSM based on digital twin and ISSA-RF, and carries out 3D visual monitoring of the running status of PMSM. In this method, the fault characteristics of PMSM stator current are extracted through Variational Mode Decomposition (VMD), the ISSA-RF fault diagnosis model is trained and the digital twin fault diagnosis system is established. The validity of the proposed fault diagnosis method is verified by simulation and experimental analysis.

2. Digital Twin Model of PMSM

2.1. Digital Twin Fault Diagnosis Framework

Digital twin aims to build a virtual entity mapped to a physical entity in the form of digitalization, and to conduct simulations and fault diagnosis concerning physical entities by combining historical data, real-time data and algorithm models [28]. As shown in Figure 2, the digital twin framework of PMSM fault diagnosis includes perception layer, transmission layer, model layer and service layer.
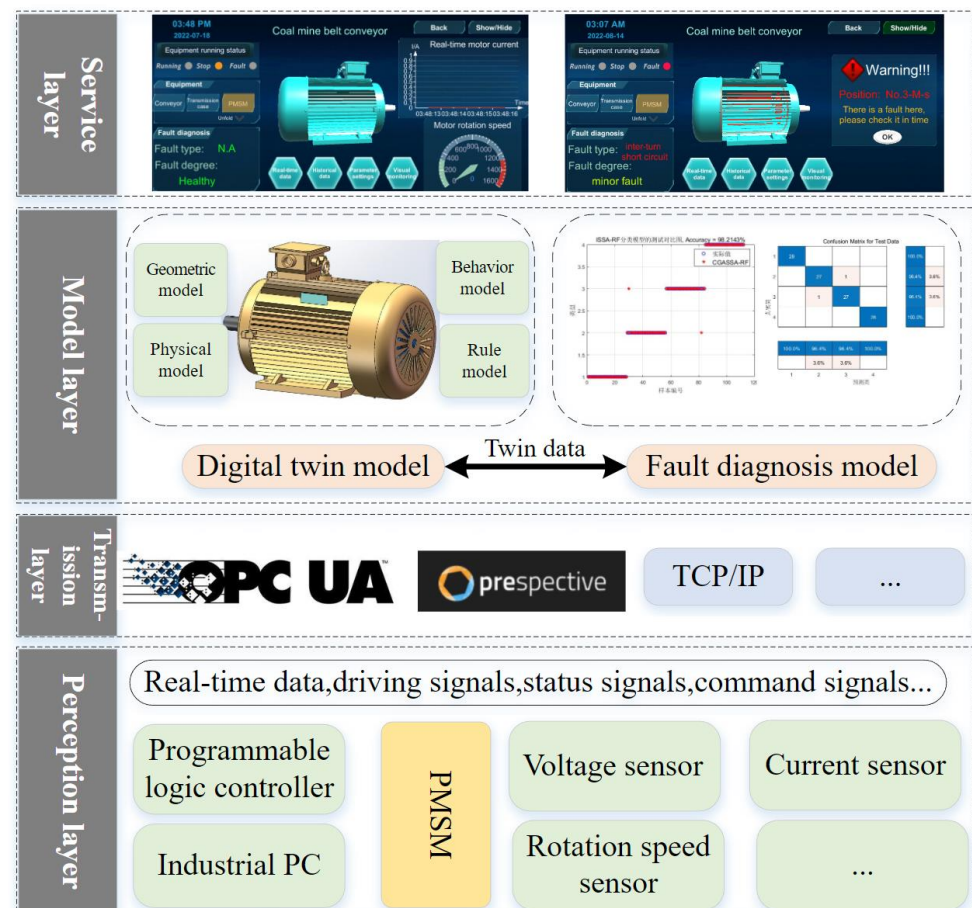

Figure 2. Permanent Magnet Synchronous Motor Fault Diagnosis Digital Twin Framework.

The function of the perception layer is to obtain the real-time data of the physical PMSM such as the data of driving signals, status models and sensors, including permanent magnet synchronous motor, sensor, programmable logic controller, etc.

The function of the transmission layer is to connect the physical entity and the virtual entity for data interaction. The commonly used communication protocols are TCP/IP, MQTT, OPC UA and so on [29]. The plug-in PREspective in Unity3D has been applied to the digital twin technology because it provides multiple industrial communication protocol interfaces and can access various simulations (such as MATLAB simulation) and realize real-time communication between digital twin and simulation software.

The model layer refers to the digital twin model and the fault diagnosis model, and the two are connected with each other through twin data. The digital twin model includes the physical model, the geometric model, the rule model and the behavior model. The fault diagnosis model trains the selected algorithm network according to the historical data or twin data of the permanent magnet synchronous motor so as to realize the fault diagnosis of the permanent magnet synchronous motor.

The service layer refers to the human–machine interaction interface, which is a visual window of the digital twin to realize the fault visualization, real-time optimization control and data management functions of the PMSM.

2.2. Construction of Twin Model of PMSM

The construction of the twin model requires the integration of the geometric model, the physical model, the rule model and the behavior model [30], which describes the twin model from multiple dimensions. Now we are going to describe the twin model of the permanent magnet synchronous motor from four dimensions.

2.2.1. Geometric Model

The geometric model describes the shape, position relationship and parent–child relationship of physical entities, etc. The geometric parameters of PMSM mainly include stator, rotor, permanent magnet, etc., which are modeled by 3Dmax, Maya and other software and imported into Unity3D for rendering [31], as shown in Figure 3.
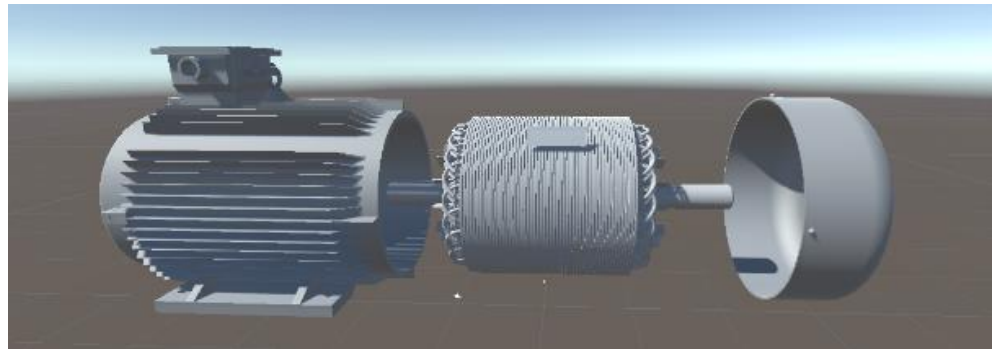
Figure 3. Geometric model.

2.2.2. Physical Model

Based on the geometric model, physical attributes of PMSM such as current, voltage, magnetic field and speed are added to the physical model to simulate the change process of physical parameters. The software commonly used are ANSYS, ABAQUS finite element analysis software, etc. [32–34].

2.2.3. Rule Model

Rule model is based on existing historical experience rules, expert knowledge rules and standard rules in related fields to enable the virtual model to restrict, deduct and diagnose fault, etc. Machine-learning algorithms can be used to mine historical data and generate new rules. As historical data evolve and time goes by, these rules will evolve and improve, improving the ability of real-time optimization, prediction and fault diagnosis of rule models.

2.2.4. Behavior Model

The behavior model describes the real-time response and behavior of PMSM under different environments and different time scales combined with its internal operating mechanism, including healthy operation behavior, failure behavior and performance degradation behavior of PMSM [35].

The PMSM fault behavior model described in this paper is as follows:

$$B_f = \left(t_f, d_f, p_f, m_f \right) \tag{1}$$

where t_f refers to the fault type of PMSM, d_f stands for the fault degree of PMSM, p_f indicates the fault position and m_f refers to the fault model. The main purpose of the behavior model is to reflect the real-time behavior of the physical entity (health behavior, fault behavior,

etc.) in virtual space, analyze and judge the collected real-time data by the rule model, obtain the real running state of the physical entity and update the behavior model to make it consistent with the running state of the physical entity.

To describe the permanent magnet synchronous motor twin model from multiple time scales and space scales, the above four models need to be assembled and fused. Thus, the permanent magnet synchronous motor twin model can be expressed as [36]:

$$\mathrm{MT_{PMSM}} = (G_{\mathrm{m}}, P_{\mathrm{m}}, R_{\mathrm{m}}, B_{\mathrm{m}}) \tag{2}$$

where $\mathrm{MT_{PMSM}}$ refers to the permanent magnet synchronous motor twin model, G_{m} is the geometric model, P_{m} is the physical model, R_{m} is the rule model and B_{m} is the behavior model.

The permanent magnet synchronous motor twin model can not only realize real-time mapping of physical entities, but also realize PMSM state monitoring through dynamic simulation of PMSM by the data-driven twin model [37]. The assembly and fusion of the permanent magnet synchronous motor twin model are shown in Figure 4. Through the data-driven $\mathrm{MT_{PMSM}}$, it is possible to determine whether the PMSM is faulty, and when a fault occurs, the fault location can be quickly located, the cause of the fault can be analyzed and the degree of equipment failure can be evaluated.
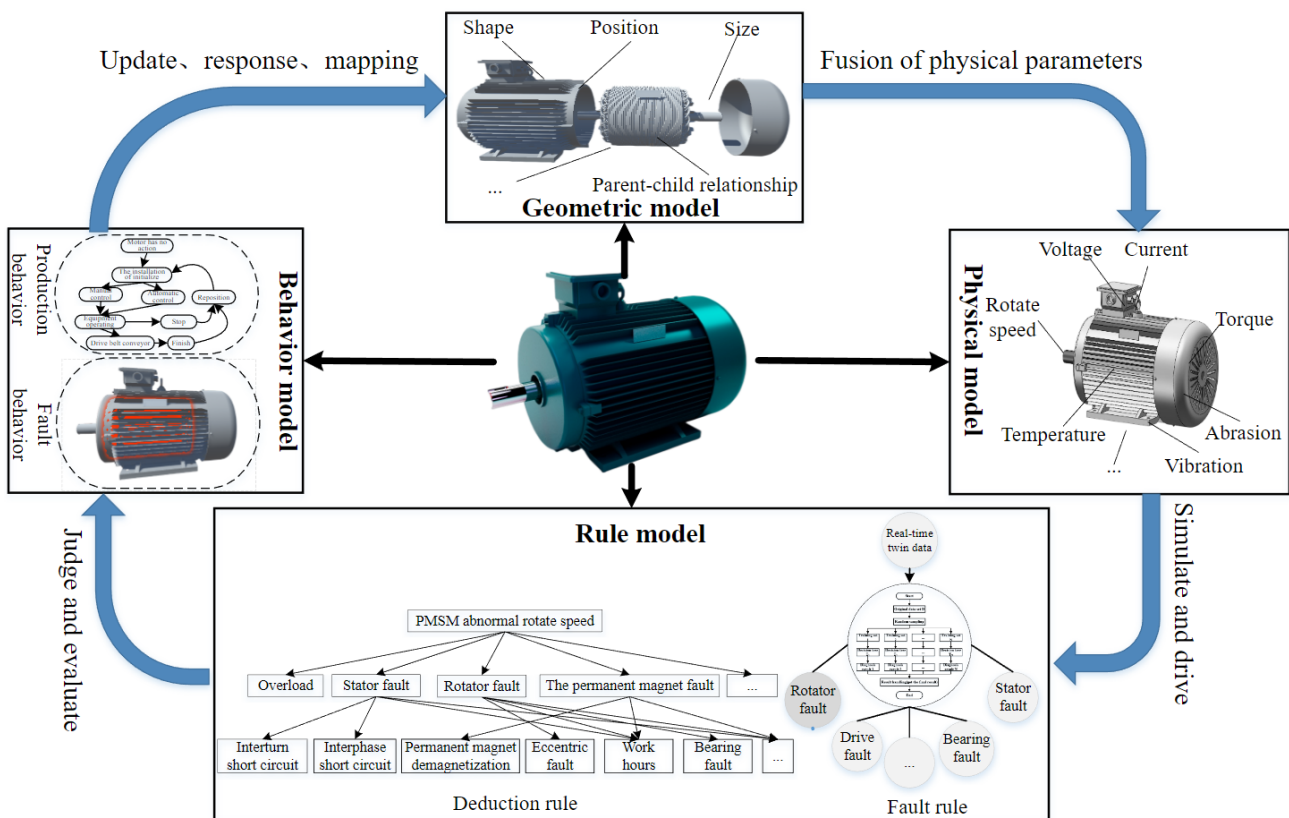

Figure 4. Multidimensional model of PMSM.

2.3. PMSM Fault Diagnosis Based on the Fusion of Data Driving and Twin Model

With the development of artificial intelligence, the fault diagnosis accuracy of PMSM by using data driving is constantly improving. However, for some faults that machine learning has not trained, accurate fault diagnosis cannot be carried out. Therefore, this paper integrates data driving and twin model to jointly realize fault diagnosis of PMSM, and adopts the twin model to conduct a consistency test on machine-learning diagnosis results, as shown in Figure 5, to dynamically, stably and accurately diagnose PMSM fault. Firstly, the machine-learning algorithm is trained and tested according to the historical

data or simulation data of PMSM, which is elaborated in Sections 3.3 and 4.1. Secondly, the real-time data of PMSM are collected through the perception layer, including driving signal, command signal, status signal, etc. Third, the data is transmitted to the model layer (machine-learning model and twin model) through the transmission layer. After the twin data is preprocessed, it is transmitted to the twin model for simulation, and simultaneously the twin data is transmitted to the data-driven machine-learning model [38]. If the diagnosis results of the two models are consistent, the fault position, fault type and fault degree are displayed in the service layer, and optimization decisions are made based on the diagnosis results and fed back to the physical entity PMSM. Otherwise, the fault database is updated, which is beneficial in terms of the machine-learning model being updated and optimized.
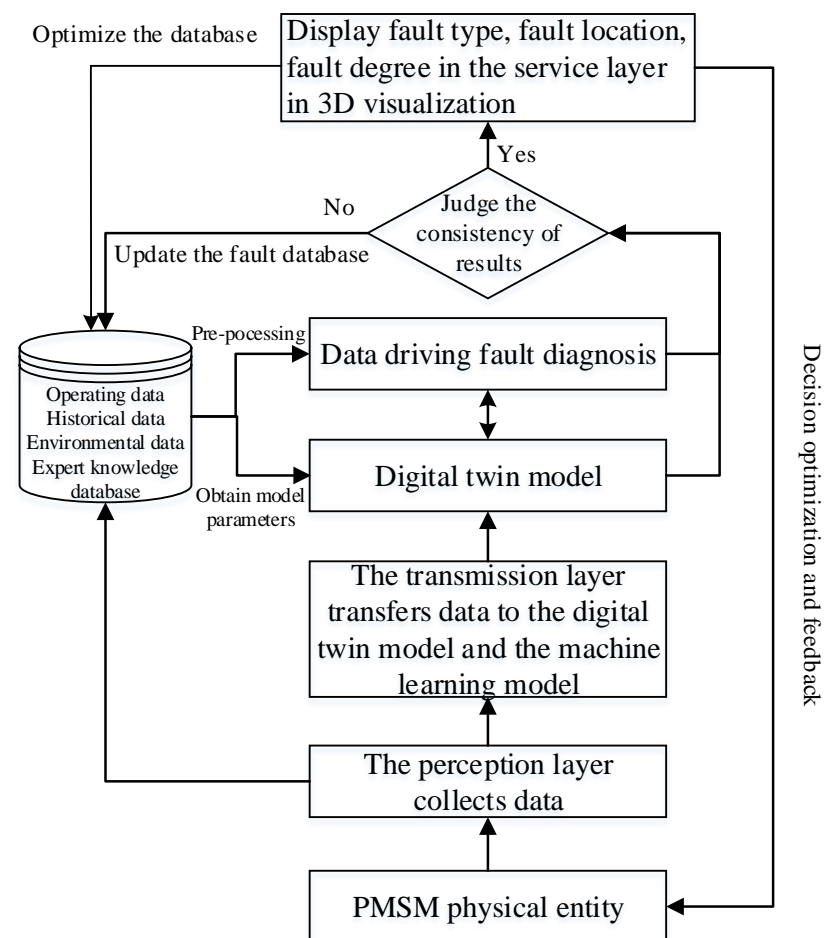
**Figure 5.** PMSM fault diagnosis frame.

Currently, machine-learning algorithms commonly used for data driving include: Support Vector Machine (SVM) [39], Long Short-Term Memory (LSTM), BP (Back Propagation) neural network, Random Forest, etc. [40]. The accuracy of the machine-learning algorithm is crucial to the method proposed in this paper. Therefore, an Improved Sparrow Search Algorithm for Optimizing Random Forest (ISSA-RF) is proposed in this paper to improve the accuracy of PMSM fault diagnosis. In this paper, the inter-turn short circuit fault of PMSM is taken as an example to verify the feasibility and effectiveness of the ISSA-RF algorithm.

2.4. Equivalent Model of PMSM Inter-Turn Short Circuit Fault

The faults of PMSMs can be divided into electrical faults, mechanical faults and permanent magnet faults. Studies show that more than 47% of motor faults are caused by electrical faults [41], among which the short circuit between stator windings is the most common electrical fault and is generally caused by high temperature, mechanical vibration

extrusion, humidity and other factors. The short circuit between PMSM turns will not only affect the motor performance, but also cause other types of faults or even damage the motor. The reason is that the short-circuit coil produces counter electromotive force in contrast to the normal coil, causing the magnetic field of the short-circuited coil to be opposite the direction of the original magnetic field. In addition, the stator windings with inter-turn short-circuit fault will produce a short-circuit current, leading to a rise of local temperature of the motor, demagnetization of the permanent magnet in the motor and further attenuation of motor performance.

Figure 6 shows the equivalent circuit model (A-phase inter-turn short circuit of three-phase PMSM) when inter-turn short circuit fault occurs in the stator winding of PMSM, in which u stands for voltage, i is the current, e is the counter electromotive force (where e_{af} is the counter electromotive force generated by the short-circuit coil), R is the resistance of the stator winding coil (where R_f is the resistance of the short-circuit branch), L is the inductance of the stator winding coil, a, b and c, respectively, correspond to the A, B and C phases of the three-phase PMSM and mutual inductance M_{ij} exists between each of the two coils (i and j are subscripts of coils).
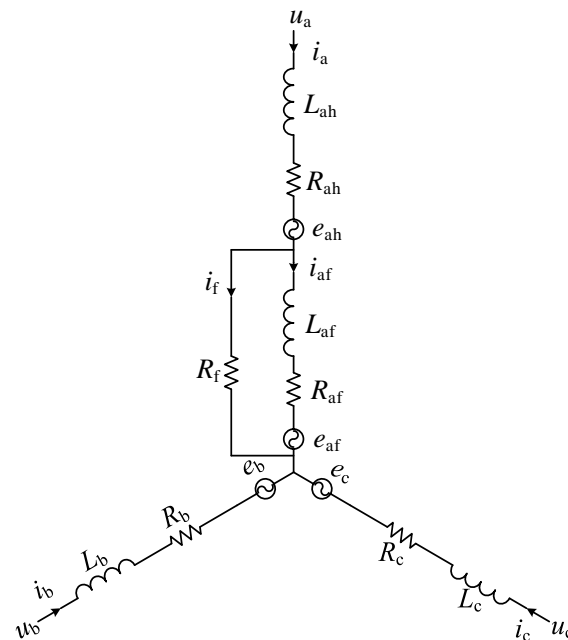
Figure 6. Equivalent circuit model of A-phase inter-turn short circuit fault of permanent magnet synchronous motor.

3. Fault Diagnosis Method Based on ISSA-RF Permanent Magnet Synchronous Motor

3.1. Random Forest Algorithm

The Random Forest (RF) algorithm is an ensemble classifier composed of multiple decision trees, and was proposed by Leo Breiman in 2001 [42]. RF improves the generalization ability and prediction accuracy of the model by increasing the difference between various classifiers [43]. Two "random" features are used to construct a decision tree to form a Random Forest: (1) bootstrap; (2) characteristics of randomly selected training samples.

As shown in Figure 7, the steps for Random Forest fault diagnosis are as follows: original data set D $= \{C_{i1}, C_{i2}, C_{i3}, \cdots, C_{iM}, Y_j\}$ (i = 1, 2, ... , n; j = 1, 2, ... , u), where M refers to the quantity of features, Y_j is the corresponding output category label under $\{C_{i1}, C_{i2}, C_{i3}, \cdots, C_{iM}\}$, and u is the quantity of category labels.

1.　N (N < n) training subsets were randomly sampled from the original data set D by the bootstrap sampling method;
2.　m features were randomly selected from M features ($m < M$) to generate a decision tree model;

3. The above steps were repeated to generate N decision trees to form a Random Forest classification model.

4. The Random Forest classification model was used to classify and diagnose the test data set, and the result of each decision tree is calculated by means of ensemble voting to get the final diagnosis result. The final result is decided by majority vote:

$$\text{Result}(x) = \text{argmax}_Y \sum_{h=1}^{N} I\{T_h(x) = Y\} \tag{3}$$

where $T_h(x)$ refers to the hth decision tree, Y is the category label and $I\{\cdot\}$ is an indicative function.
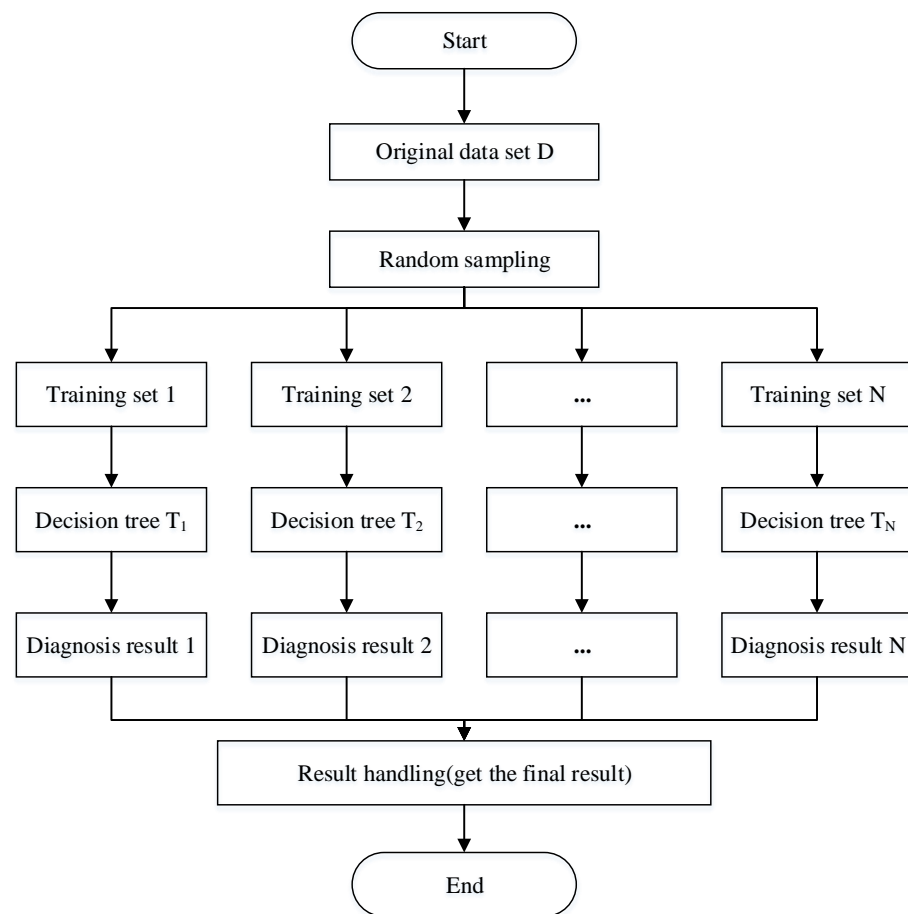
Figure 7. Random Forest Classification Flowchart.

3.2. Strategy to Improve the Sparrow Search Algorithm

3.2.1. Sparrow Search Algorithm

Sparrow Search Algorithm (SSA) is a new intelligent search algorithm proposed by Xue Jiankai in 2020 [44] that divides sparrows into discoverers and followers according to the fitness value in the foraging process. The discoverers have higher fitness values and will preferentially obtain food in the process of foraging. Moreover, they have a wider search range and will guide the followers to forage and search. For the followers, they will follow the discoverer with the best fitness value to forage and search. To obtain better food, they will monitor whether the discoverer finds better food, and may compete for the discoverer's food to increase their own predation rate. The identity of discoverer and follower is dynamic, but the proportions of discoverer and follower to the whole population are fixed. To ensure the safe foraging of the population, each generation randomly selects 10% to 20% sparrows from the whole population as vigilantes to monitor the foraging area.

They immediately send alerting signals when sensing risks, and the sparrow population will move to a safe position or engage in anti-predation behavior.

The location updating formulae of discoverer, follower and vigilante are, respectively, as follows:

Suppose there are n sparrows in the population that search in d-dimension space. The location of the ith sparrow can be expressed as $X_i = [x_{i1}, x_{i2}, \cdots, x_{id}]$, where $i = 1, 2, \cdots, n$ and its fitness value can be expressed as $f_i = f[x_{i1}, x_{i2}, \cdots, x_{id}]$.

The location-updating formula of the discoverer is:

$$X_{i,d}^{t+1} = \begin{cases} X_{i,d}^t \cdot \exp(-\frac{i}{\alpha \cdot \text{iter}_{\max}}) & R_2 < ST \\ X_{i,j}^t + QL & R_2 \geq ST \end{cases} \tag{4}$$

where $X_{i,d}^t$ refers to the d-dimension location information of the ith sparrow in the tth generation, α is a random number and $\alpha \in (0, 1)$, $\text{iter}_{\max}$ is the quantity of the maximum iteration, Q is a random number that follows a normal distribution, L is a $1 \times d$ matrix with all its elements equal to 1, $R_2 \in [0, 1]$ refers to the alerting value, and $ST \in [0.5, 1]$ refers to the safety value. When $R_2 < ST$, it means the foraging environment is good for sparrows and there is no predator. Conversely, when $R_2 \geq ST$, it means predator(s) is (are) found by some sparrows in the population and alerts are sent out.

The location updating formula of the follower is:

$$X_{i,d}^{t+1} = \begin{cases} Q \cdot \exp(\frac{X_w^t - X_{i,d}^t}{i^2}) & , i > \frac{n}{2} \\ X_b^{t+1} + \left| X_{i,d}^t - X_b^{t+1} \right| \cdot A^+ \cdot L & , i \leq \frac{n}{2} \end{cases} \tag{5}$$

where X_b and X_w, respectively, refer to the best location and the worst location in the sparrow population; A is a $1 \times d$ matrix in which each element is randomly assigned with value 1 or -1, $A^+ = A^T(AA^T)^{-1}$. When $i > \frac{n}{2}$, the ith low-fitness follower will have no food to move to other places for more energy. When $i \leq \frac{n}{2}$, the ith follower forages randomly near the currently best location of the population.

The location updating formula of the vigilante is:

$$X_{i,d}^{t+1} = \begin{cases} X_b^t + \beta \left| X_{i,d}^t - X_b^t \right| & , f_i > f_b \\ X_{i,d}^t + \gamma \left[\frac{|X_{i,d}^t - X_w^t|}{(f_i - f_w) + \delta} \right] & , f_i = f_b \end{cases} \tag{6}$$

where β is the step size control parameter and is a random number that follows the standard normal distribution, δ is the smallest constant to avoid having a zero denominator, $\gamma \in [-1, 1]$ is a random number and f_b and f_w are, respectively, the current best and worst fitness values. When $f_i > f_b$, the sparrow is at the edge of the population and vulnerable to predators; when $f_i = f_b$, the sparrow is in the middle of the population and needs to move closer to other sparrows to avoid attack.

3.2.2. Strategy to Improve the SSA

(1) Tent chaotic mapping initialization population

Chaos is a nonlinear natural phenomenon, and the chaotic motions feature randomness, regularity and ergodicity. The existing chaotic maps include Circle chaotic map, Logistic chaotic map, Tent chaotic map, etc., which are widely used in optimization search algorithms. The chaotic value distribution of the Circle chaotic map is uneven, and the values in the interval [0.2, 0.6] are relatively dense [45] while the values of the Logistic chaotic map are relatively dense in the intervals [0, 0.05] and [0.95, 1], proving to be low in the middle and high on both sides [46]. The distribution of Tent chaotic map in the

interval [0, 1] is more uniform with a faster iteration speed [47]. Therefore, in this paper, Tent chaotic map is used to initialize the sparrow population. The expression is as follows:

$$x_{t+1} = \begin{cases} \frac{x_t}{\beta} & 0 \le x_t < \beta \\ \frac{1-x_t}{1-\beta} & \beta \le x_t \le 1 \end{cases} \tag{7}$$

where $\beta \in (0, 1)$, and $\beta = 0.7$ in this paper. The specific mapping expression is:

$$x_{t+1} = \begin{cases} \frac{10x_t}{7} & 0 \le x_t < 0.7 \\ \frac{10-10x_t}{3} & 0.7 \le x_t \le 1 \end{cases} \tag{8}$$

The basic sparrow search algorithm will randomly initialize the position of the sparrow population, resulting in uneven distribution of individual positions within the sparrow population and low population diversity. By introducing the Tent chaotic map to initialize the population distribution of the SSA algorithm, x_{new} is obtained, which increases the diversity of the sparrow population and speeds up the convergence of the SSA algorithm. It can be expressed by the following formula:

$$x_{new} = lb + (ub - lb)x_d \tag{9}$$

where x_{new} is the new population obtained through the use of the Tent chaotic map; ub and lb are the upper and lower limits of the variable x; and x_d is the Tent chaos sequence.

(2) Genetic algorithm—crossover and mutation

To increase the population diversity and improve the accuracy of the sparrow search algorithm, the crossover mutation of the genetic idea is introduced. Firstly, binary coding is adopted for the discoverer individuals in the sparrow population, and the individual extreme value and the population extreme value are crossed to obtain a better next generation. The size of the crossover probability Pc will affect the optimization ability of the algorithm. If the selection of Pc is too small, the speed of generating new individuals will be slower. If the selection of Pc is too large, the speed of generating new individuals will be too fast and the number will be too large. It also increases the likelihood of disrupting genetic patterns and affecting the structure of the population that produces superior individuals; secondly, an individual is randomly selected in the discoverer population to mutate the gene of the selected individual with a certain mutation probability Pm to generate a new individual. The size of the mutation probability Pm will affect the performance and convergence of the algorithm. If the value of Pm is too small, it will be difficult to generate new individuals, resulting in the loss of many excellent genes and insufficient diversity of the population. If the value of Pm is too large, it will become a pure random search algorithm, which is not conducive to the convergence of the algorithm [48]. Finally, after relevant experimental research, this paper selects Pc = 0.8, Pm = 0.1 to cross-mutate the sparrow population.

(3) T-distribution

T-distribution, also known as student distribution, is a statistical distribution form proposed by Gosset, a mathematical statistician [49]. The probability density function of T-distribution obeying degree of freedom n is:

$$p_t(x) = \frac{\Gamma\left(\frac{n+1}{2}\right)}{\sqrt{n\pi} \cdot \Gamma\left(\frac{n}{2}\right)} \cdot \left(1 + \frac{x^2}{n}\right)^{-\frac{n+1}{2}} \quad -\infty < x < +\infty \tag{10}$$

T-distribution is the intermediate form of Gaussian distribution and Cauchy distribution. When the degree of freedom $n = 1$, T-distribution is the standard Cauchy distribution with strong global search ability. When the degree of freedom $n \to \infty$, T-distribution is the Gaussian distribution with strong local search ability. Therefore, selecting the proper n

value, the T-distribution can play to the best of both. The variation process of T-distribution with iteration number iter as the degree of freedom *n* can be written as follows:

$$x_i(new) = x_i(old) + x_i(old)t_{\text{iter}} \tag{11}$$

where $x_i(new)$ and $x_i(old)$ are, respectively, the new position of the *i*th sparrow after mutation and the original position before mutation, t_{iter} refers to the T-distribution that relates to the iteration number. By introducing T-distribution, the global search ability can be enhanced in the early stage of iteration, and the local search ability can be better in the late stage of iteration. In addition, the convergence speed of the algorithm can be accelerated.

(4) Simulated annealing mechanism

To enhance the ability of the SSA to jump out of the local optimal solution and find the global optimal solution quickly, a simulated annealing mechanism is introduced. Simulated annealing is the process of simulating the annealing of solid substances in physics [50], of which the cooling mode is as follows:

$$T_{x+1} = \lambda T_x \tag{12}$$

where T refers to the annealing temperature that decides the probability of a sparrow receiving the new location, λ is the annealing coefficient and $\lambda \in [0.9, 1]$. When the fitness value of the new location f_{new} is better than the current optimal fitness value f_o, the original one is directly replaced; otherwise, the Metropolis criterion needs to be followed to judge as below:

$$\exp\left(-\frac{f_{new} - f_o}{T}\right) \geq rand(0, 1) \tag{13}$$

If the formula is true, the new location will be accepted; otherwise, it will be rejected.

3.2.3. Improved Sparrow Search Algorithm Test

In this paper, four unimodals and four multimodals are selected as test functions (as shown in Table 1, the information of the test function includes function type, function formula, dimension, range and optimal value), and the ISSA Algorithm, the Whale Optimization Algorithm (WOA), the Grey Wolf Optimization Algorithm (GWO), the Particle Swarm Optimization (PSO) and the SSA algorithm are compared. Each algorithm is run 50 times with a population size of 30 to calculate the worst value, the optimal value, the mean value and the standard deviation of those five optimization algorithms as evaluation indexes. Specific parameter settings of each optimization algorithm are as follows: WOA parameter settings: a reduces from 2 to 0 linearly, $p = 0.5$, $b = 1$; GWO parameter settings: a decreases linearly from 2 to 0; PSO parameter settings: $\omega_{max} = 0.9$, $\omega_{min} = 0.2$, $c_1 = 2$, $c_2 = 2$; SSA parameter settings: $ST = 0.6$, $PD = 0.7$, $SD = 0.2$.

The experimental results in Table 2 (the data in bold in the table are the best values for that group) and Figure 8 show that ISSA achieved better optimization results than the other four algorithms in the optimization experiments of the eight test functions (unimodal and multimodal) selected. In F_1 and F_4, the optimization effects of ISSA were far better than those of other optimization algorithms, with accurate optimization accuracy and fast convergence speed. In F_2 and F_3, ISSA improved the optimal value by more than 10 orders of magnitude compared with PSO, WOA and GWO, and improved the mean value and the standard deviation by about 5 orders of magnitude. Although the SSA algorithm also achieved good optimization effect, it was still not as accurate as ISSA. Therefore, for the unimodal test functions $F_1 \sim F_4$, the optimal value and the average value of the ISSA algorithm are the closest to the theoretical optimal value of the test function, and the standard deviation of the ISSA algorithm is the smallest. This is because the ISSA algorithm introduces the Tent chaotic map and crossover mutation, which increases the diversity of the sparrow population, improves the convergence speed of the algorithm and results in a strong global search ability of the algorithm. In the multimodal and low-dimensional test functions F_5 and F_6, although the five optimization algorithms all find the

same optimal value, ISSA is more stable and converges faster than the other four algorithms. In the multimodal and high-dimensional test functions F_7 and F_8, the three optimization algorithms SSA, ISSA and WOA have all achieved good results, but the standard deviation of ISSA is the smallest, indicating that the ISSA optimization algorithm is more stable and robust, and can jump out of the local optimal solution. In F_7, both SSA and ISSA find the optimal value stably, which shows the superiority of the sparrow search algorithm itself. Therefore, for the multimodal test functions $F_5 \sim F_8$, the average value of the ISSA algorithm is closer to the optimal value of the test function, which reflects that the ISSA algorithm has the highest accuracy in finding the optimal solution. In addition, with the smallest standard deviation, the ISSA algorithm has strong stability and robustness, and fast convergence speed according to the test function convergence curve (e–h). This is mainly because the ISSA algorithm introduces two strategies, T-distribution and simulated annealing. The T-distribution strategy enhances the global search ability in the early stage of the algorithm and the local search ability in the later iteration, while the simulated annealing strategy strengthens the algorithm's ability to jump out of the local optimal solution.

**Table 1.** Test function information.

| Function Type	Function Formula	Dimension	Range	The Optimum
Unimodal	$F_1(x) = \sum_{i=1}^{n} x_i^2$	30	$[-100, 100]$	0
Unimodal	$F_2(x) = \sum_{i=1}^{n-1} \left[100\left(x_{i+1} - x_i^2\right)^2 + (x_i - 1)^2 \right]$	30	$[-30, 30]$	0
Unimodal	$F_3(x) = \sum_{i=1}^{n} \left([x_i + 0.5]\right)^2$	30	$[-100, 100]$	0
Unimodal	$F_4(x) = \sum_{i=1}^{n} |x_i| + \prod_{i=1}^{n} |x_i|$	30	$[-10, 10]$	0
Multimodal	$F_5(x) = -\sum_{i=1}^{4} c_i \exp\left(-\sum_{j=1}^{6} a_{ij}\left(x_j - p_{ij}\right)^2 \right)$	6	$[0, 1]$	-3.32
Multimodal	$F_6(x) = \left(\frac{1}{500} + \sum_{j=1}^{25} \frac{1}{j + \sum_{i=1}^{2} (x_i - a_{ij})^6} \right)^{-1}$	2	$[-65, 65]$	1
Multimodal	$F_7(x) = -20 \exp\left(-0.2\sqrt{\frac{1}{n}\sum_{i=1}^{n} x_i^2} \right) - \exp\left(\frac{1}{n}\sum_{i=1}^{n} \cos(2\pi x_i) \right) + 20 + e$	30	$[-32, 32]$	0
Multimodal	$F_8(x) = \sum_{i=1}^{n} -x_i \sin\left(\sqrt{|x_i|} \right)$	30	$[-500, 500]$	$-12{,}569.487$

Table 2. Test function result comparison.

Function	Algorithm	The Worst Value	The Optimal Value	The Mean Value	Standard Deviation
F_1	WOA	1.1026E−150	3.7848E−170	3.4927E−152	1.739E−151
	GWO	7.8671E−58	1.2739E−61	5.768E−59	1.2134E−58
	PSO	1.5351	0.28415	0.80961	0.29399
	SSA	1.5731E−39	**0.00E+00**	3.1461E−41	2.2246E−40
	ISSA	**0.00E+00**	**0.00E+00**	**0.00E+00**	**0.00E+00**
F_2	WOA	28.7271	26.1422	27.0898	0.48525
	GWO	28.5395	25.1895	26.9658	0.73291
	PSO	1759.8402	90.1762	329.1056	338.0528
	SSA	0.00087056	1.9429E−10	2.6087E−05	0.00012261
	ISSA	**0.000128**	**1.394E−11**	**1.6906E−05**	**2.8937E−05**
F_3	WOA	0.51245	0.0096724	0.11545	0.1205
	GWO	1.4982	1.4252E−05	0.6006	0.3716
	PSO	2.2191	0.19723	0.99605	0.40937
	SSA	2.4322E−06	1.5397E−12	2.1759E−07	4.9544E−07
	ISSA	**6.5149E−08**	**9.7579E−15**	**8.2053E−09**	**1.4792E−08**
F_4	WOA	4.2731E−101	5.6882E−117	9.3139E−103	6.0485E−102
	GWO	6.381E−34	5.7026E−36	1.1818E−34	1.3682E−34
	PSO	8.5704	1.3881	5.2468	1.72
	SSA	4.8452E−21	**0.00E+00**	9.7027E−23	6.852E−22
	ISSA	**0.00E+00**	**0.00E+00**	**0.00E+00**	**0.00E+00**
F_5	WOA	−2.6381	−3.322	−3.2193	0.13087
	GWO	−3.0204	−3.322	−3.2575	0.083307
	PSO	−2.6381	−3.322	−3.1448	0.1741
	SSA	−3.1354	−3.322	−3.2633	0.071025
	ISSA	**−3.2031**	**−3.322**	**−3.2459**	**0.057648**

Table 2. *Cont.*

Function	Algorithm	The Worst Value	The Optimal Value	The Mean Value	Standard Deviation
F_6	WOA	10.7632	**0.998**	2.1992	2.3476
	GWO	12.6705	**0.998**	4.3642	4.29
	PSO	5.9288	**0.998**	1.7324	0.91169
	SSA	12.6705	**0.998**	9.8475	4.6552
	ISSA	**0.998**	**0.998**	**0.998**	**1.2285E−16**
F_7	WOA	7.9936E−15	**8.8818E−16**	3.8725E−15	2.1959E−15
	GWO	2.2204E−14	1.1546E−14	1.581E−14	2.4864E−15
	PSO	7.5458	2.429	3.704	0.8883
	SSA	**8.8818E−16**	**8.8818E−16**	**8.8818E−16**	**0.00E+00**
	ISSA	**8.8818E−16**	**8.8818E−16**	**8.8818E−16**	**0.00E+00**
F_8	WOA	−7676.802	−12,569.3926	−10,984.6355	1683.268
	GWO	−3322.8588	−7398.1366	−5900.4489	837.2153
	PSO	−2411.375	−4956.3865	−3179.2495	**511.3516**
	SSA	−5410.3787	−12569.4857	−9368.4539	2448.4265
	ISSA	**−10,102.0186**	**−12,569.4866**	**−11,565.6683**	786.8091
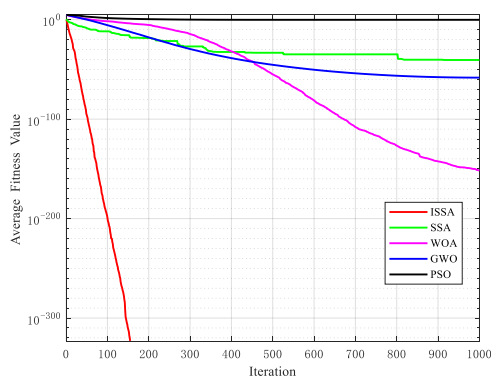
(**a**)
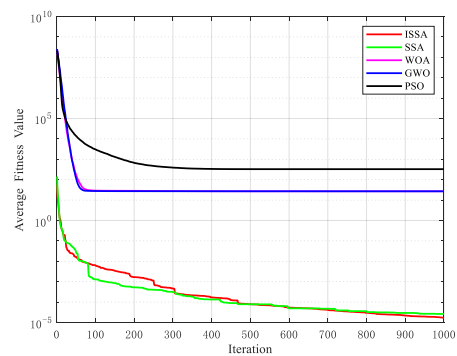
(**b**)

(**c**)

(**d**)

(**e**)

(**f**)

Figure 8. *Cont.*

(**g**)

(**h**)
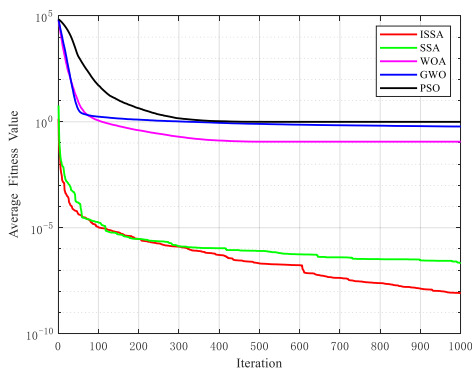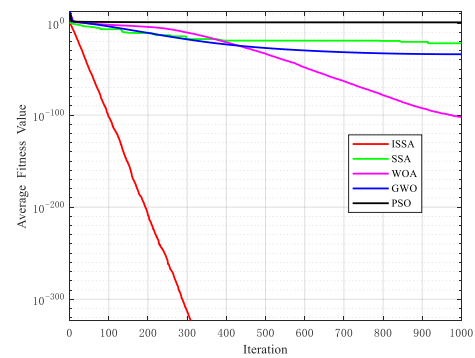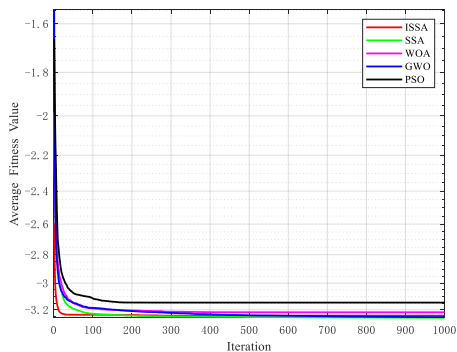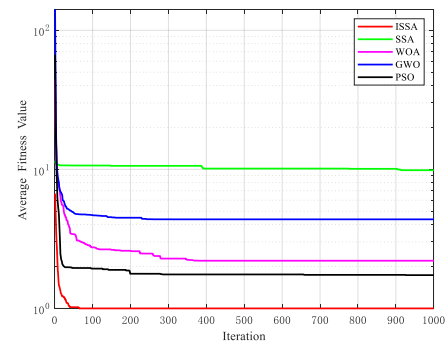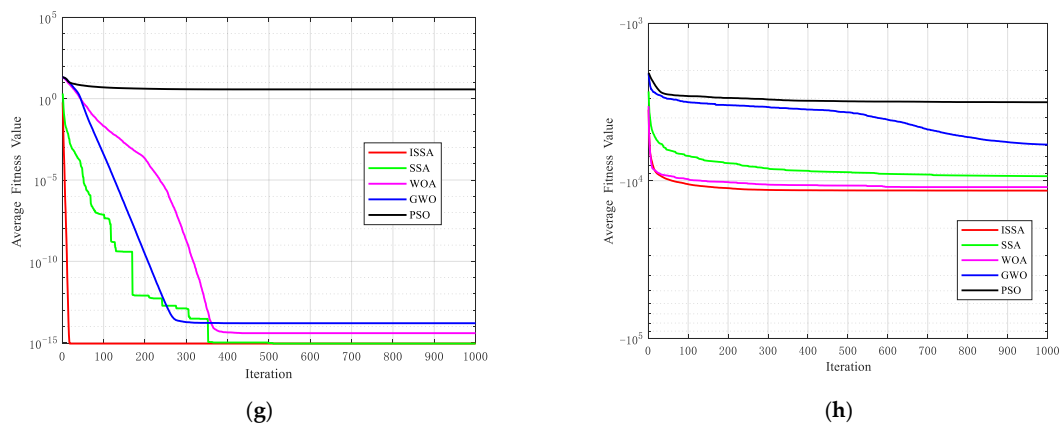
Figure 8. Test Function Convergence Plot. (**a**) F_1; (**b**) F_2; (**c**) F_3; (**d**) F_4; (**e**) F_5; (**f**) F_6; (**g**) F_7; (**h**) F_8.

To sum up, compared with other intelligence algorithms, the ISSA algorithm has the following advantages: ① it has higher solution accuracy and efficiency; ② it has strong stability and robustness; ③ it can jump out of the local optimal solution and converge quickly. Therefore, using the improved sparrow search algorithm to optimize the parameters of Random Forest is superior to using other optimization algorithms, thereby improving the accuracy of Random Forest fault diagnosis.

3.3. Fault Diagnosis Process of ISSA-RF

The accuracy of RF classification depends on the number of decision trees and the number of features at each node. This paper uses ISSA to optimize the above two variable parameters. As shown in Algorithm 1, selecting the RF model error rate as the fitness function, the fault diagnosis process of ISSA-RF is:

Algorithm: ISSA-RF.

---

1. Normalize data and divide training set ($C_{i\text{-}train}$, $Y_{j\text{-}train}$) and test set ($C_{i\text{-}test}$, $Y_{j\text{-}test}$)
2. **Input**: set the initial algorithm parameters   N: Population size
PD: Proportion of the discoverer   SD: Proportion of the vigilante
Iter-max: Maximum iteration number
3. **Training period**
Step 1: introduce the Tent mapping initial sparrow population according to Formulae (9);
Step 2: update locations according to Formulae (4)–(6) and get the optimal population X;
Step 3: obtain the population pop1 according to the crossover and mutation in the genetic ideas;
Step 4: obtain the population pop2 according to the T-distribution;
Step 5: obtain the population pop3 according to the simulated annealing;
Step 6: new X = [X pop1 pop2 pop3];
Step 7: calculate the fitness value of new population $f1$, then sort ($f1$);
Step 8: select N sparrows with higher fitness values and update the global optimal individuals, and then carry out iteration;
Step 9: check whether the stop conditions are met. If yes, exit and output the best parameters. Otherwise, perform Steps 1 to 8 again;
Step 10: train the RF classifier as per the acquired optimal parameters mtry and ntree;
Testing Period:
Step 11: test data set $C_{i\text{-}test}$
4. **Output:** label of the test data set $Y_{j\text{-}test}$

---

4. Experiment and Discussion
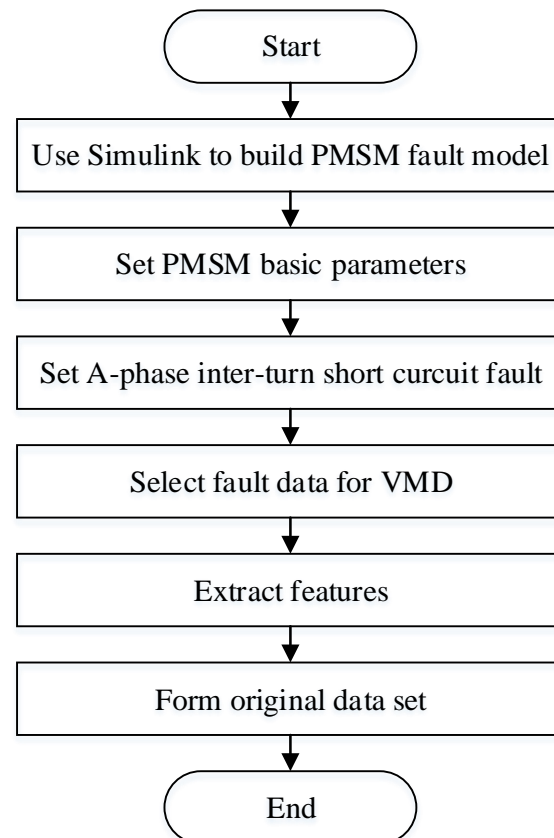
4.1. Simulation Experimental Data

The experimental environment for this paper is the Windows10 system, with a 16G running memory and a 2.90 GHz CPU. The programming language is MatlabR2021b. Through MATLAB/Simulink, the PMSM fault simulation model is built for analysis, and four types of inter-turn short-circuit fault are set up: "healthy", "minor fault", "medium

fault" and "serious fault". PMSM fault occurs 0.3 s after the start of the system. The main PMSM parameters are shown in Table 3.

Table 3. Permanent magnet synchronous motor parameters.

Variable	Value
D-axis inductance/H	0.835×10^{-3}
Q-axis inductance/H	0.835×10^{-3}
Permanent magnet flux linkage/Wb	0.152
Moment of inertia/kg · m²	0.036
Number of pole pairs	3

As shown in Figure 9, an A-phase inter-turn short circuit is taken as an example and fault data are acquired by setting different fault degrees. The data of each type are in a $15,001 \times 4$ matrix with four columns of time, A-phase current, B-phase current and C-phase current, respectively. The data of some faults that occur 0.3 s after the start running of the system are selected and the signals are decomposed by using VMD to extract the features of fault signals. Ten features are extracted in this paper, and the labels in one column include: 1 = healthy, 2 = minor fault; 3 = medium fault; 4 = serious fault. The size of the original data set is a 560×11 matrix. The data sets of the PMSM inter-turn short circuit are divided into a training set and a test set to be trained in the ISSA-RF model according to the proportion of 8:2, as shown in Table 4.

Figure 9. Building a Dataset Flowchart.

**Table 4.** Experimental data sheet.

| Label	Fault Type	Training Sample Size	Test Sample Number
1	Healthy	112	28
2	Minor fault	112	28
3	Medium fault	112	28
4	Serious fault	112	28

4.2. Results Validation

To verify the effectiveness and superiority of the improved algorithm ISSA-RF, another four algorithms, including RF, SSA-RF, BP (Back Propagation) neural network and Support Vector Machine (SVM) are, respectively, run in the same environment as ISSA-RF. The results of the fault diagnosis of 112 samples are shown in Table 5 and Figure 10.

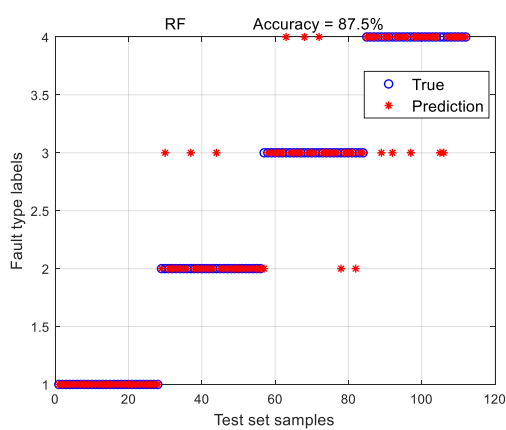**Table 5.** Comparison of Fault Diagnosis Results of Each Algorithm.

Algorithm	Test Sample Quantity	Number of Misdiagnosis	Accuracy/%
BP	112	14	87.5
SVM	112	13	88.3929
RF	112	14	87.5
SSA-RF	112	6	94.6429
ISSA-RF	112	2	98.2143
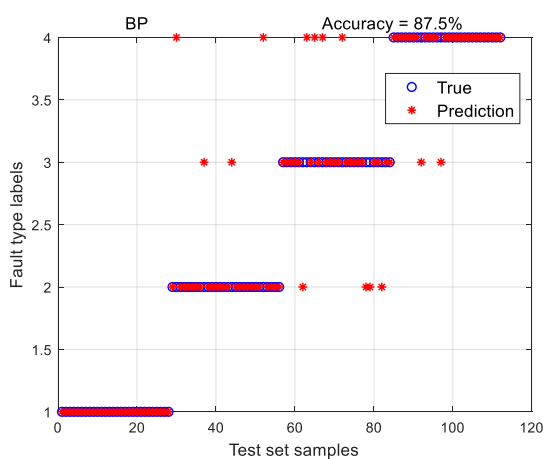
(**a**)

(**b**)

(**c**)

(**d**)

Figure 10. *Cont.*

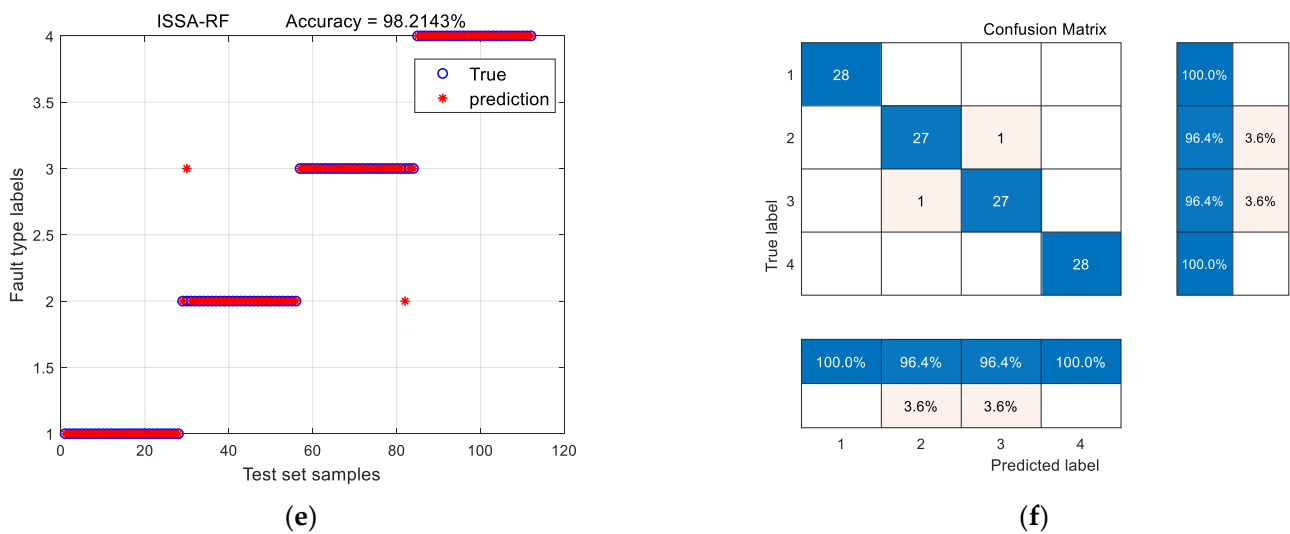**(e)**

(f)
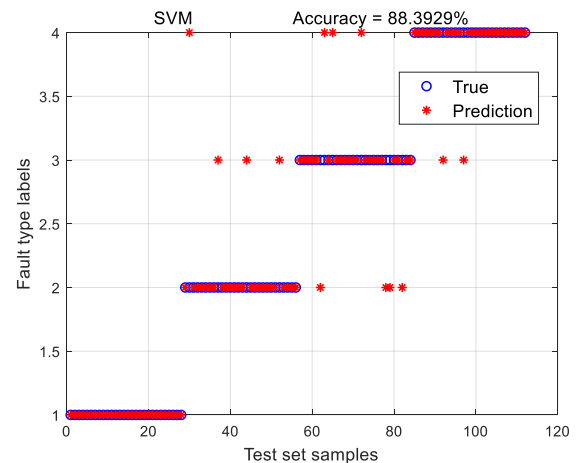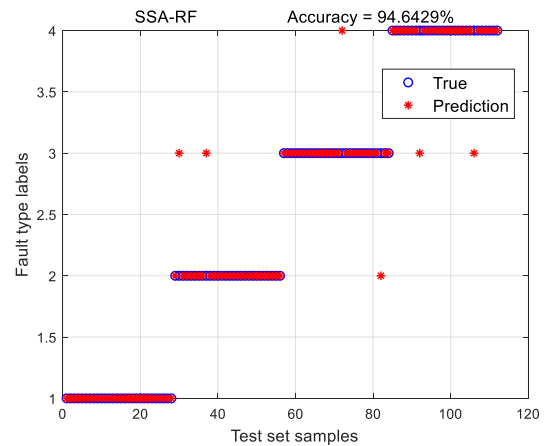
Figure 10. Actual and predicted classification results of each algorithm. (**a**) BP; (**b**) SVM; (**c**) RF; (**d**) SSA-RF; (**e**) ISSA-RF; (**f**) ISSA-RF confusion.

As can be seen from Table 5, compared with the other four fault diagnosis models, the ISSA-RF fault diagnosis model proposed in this paper performs better, and the accuracy rate in the test set reaches 98.2134%. ISSA-RF is about 10% more accurate than the three algorithms BP, SVM and RF, and about 4% more accurate than the SSA-RF algorithm.

As shown in Figure 10, the five classification models BP, SVM, RF, SSA-RF and ISSA-RF can all distinguish fault or health by PMSM. However, for the accurate classification of "minor fault", "medium fault" and "serious fault" in PMSM, due to partial similar feature fitting between faults, the accuracy rate of each algorithm is reduced. In particular, as can be seen from Figure 11, because the features of "medium fault" are partially fitted with those of "minor fault" and "serious fault", the algorithm model will incorrectly diagnose "medium fault" of PMSM as the other two kinds of fault. However, ISSA-RF is more accurate in dividing faults, and only two misdiagnoses exist. The confusion matrix of the ISSA-RF algorithm is shown in Figure 10f, which verifies the superiority of ISSA-RF against the other four algorithm models, and the superiority and feasibility of this algorithm.
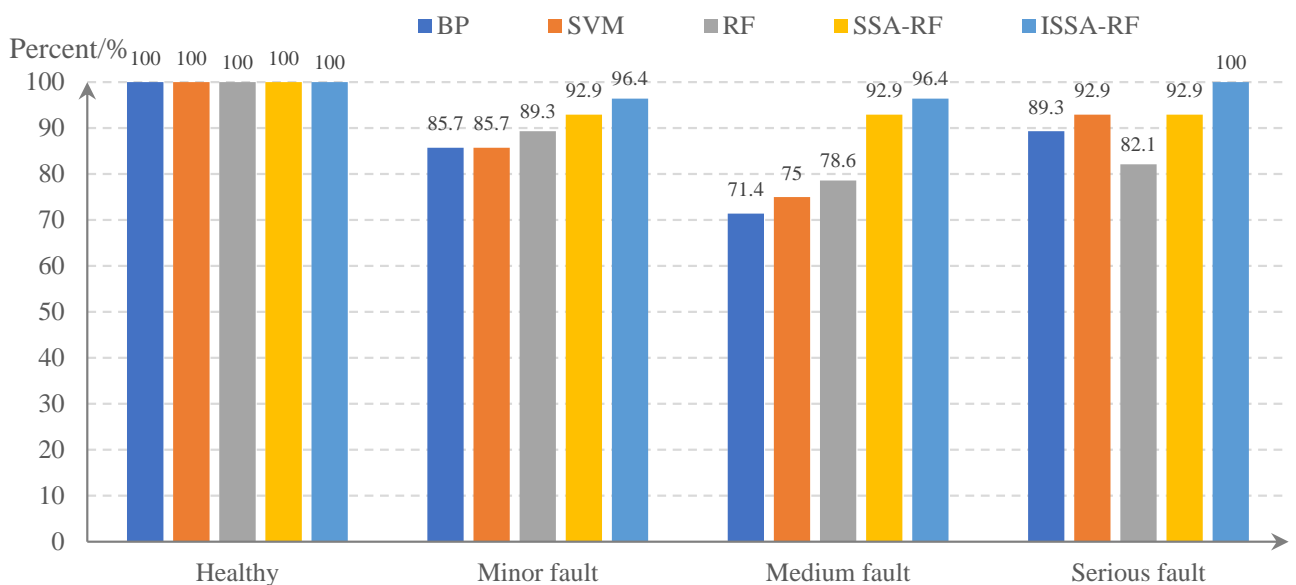
Figure 11. Specific accuracy of different fault degrees (unit: %).

4.3. Digital Twin Visualization Interface

The digital twin technology can be used for fault diagnosis and 3D visual monitoring of coal mine belt conveyor, and the real-time data collected can be transmitted to the digital twin system through the OPC UA communication protocol [51]. Real-time mapping between physical entity and twin entities can be realized through the interactive transmission of data. According to the twin data of the physical entity, the twin system will diagnose the equipment fault in combination with the ISSA-RF fault diagnosis model, the fault diagnosis results will be visualized in the twin system and the detected fault positions will be highlighted in the twin model.

As shown in Figure 12, this interface can display the running state, health condition, parameter setting and visual monitoring of the motor. Visual monitoring includes: (1) data visualization; (2) model visualization. Data visualization is to visually display the real-time data of the equipment in the form of charts. For example, the real-time current data of the motor is displayed in a line chart; the abscissa is the real time and the ordinate is the real-time current of the motor, and its unit length changes with the current. Model visualization displays the running and working status of the physical entity in real time. Meanwhile, the digital twin system will save the obtained twin data in the database, which is conducive to updating and optimizing the Random Forest fault diagnosis model in the future. As shown in Figure 13, when a device failure is detected, the digital twin system changes the device's operating status to "Fault", displays the diagnosis results in the interface and highlights the fault location on the digital twin model. In addition, a pop-up warning window displays the device number corresponding to the faulty device in the physical world to remind the staff to check the fault in time. When the staff clicks the "OK" button in the warning window, the hidden real-time current data and rotate speed of the motor will be displayed again. At this time, the staff can quickly locate the specific part and the type of the fault by viewing the Exploded View of the motor to repair or replace the part according to the severity of the failure, which improves the efficiency and safety of real-time production.
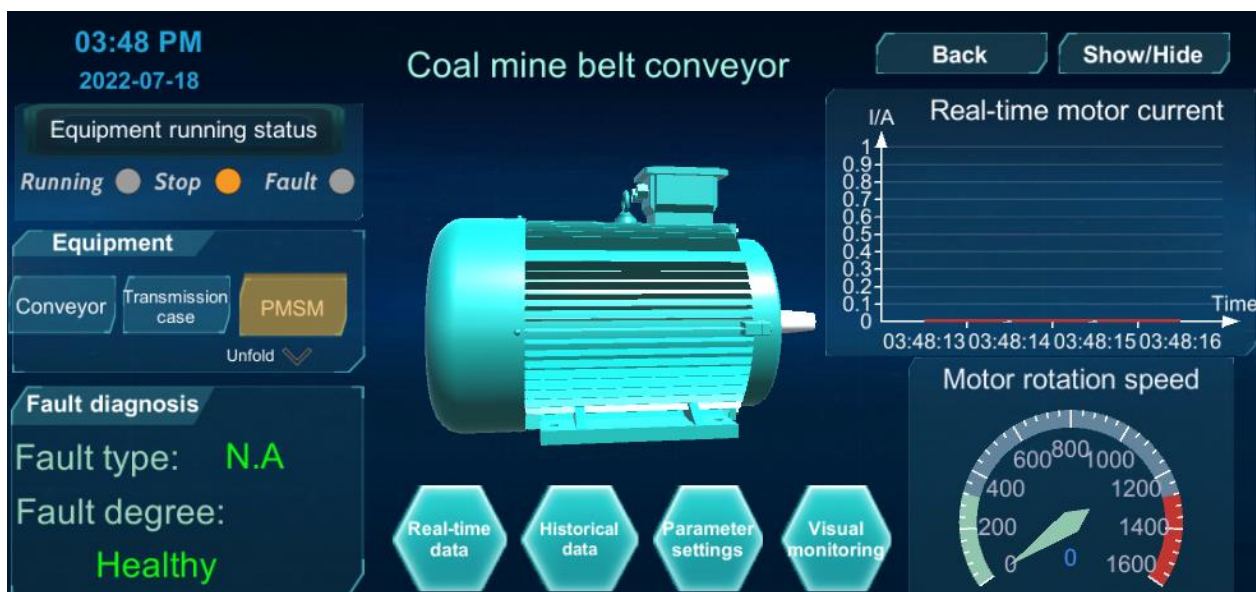

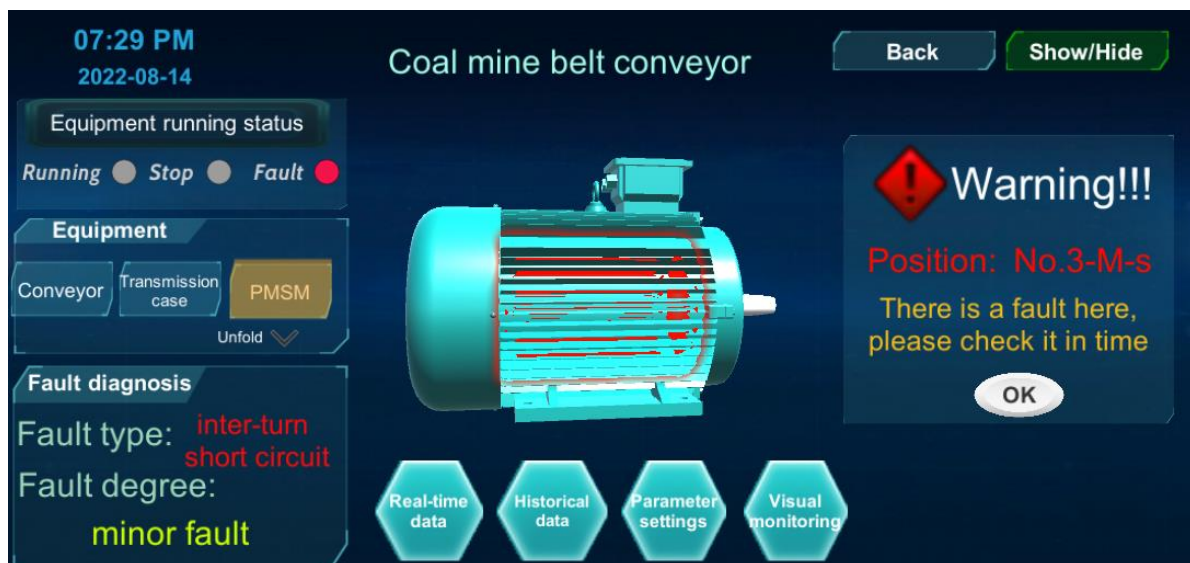**Figure 12.** Digital twin visualization interface.

Figure 13. Digital twin fault diagnosis interface.

5. Conclusions

The fault diagnosis method of PMSM based on digital twin and ISSA-RF is to diagnose the health condition of PMSM by constructing the digital twin model of PMSM and the ISSA-RF fault diagnosis model.

(1) In this paper, an improved sparrow search algorithm optimized Random Forest (ISSA-RF) method was proposed to realize the fault diagnosis of PMSM. Through simulation and feature extraction of PMSM fault data, the accuracy of the ISSA-RF diagnosis model was 98.2134%, and experimental results show that ISSA-RF is feasible and effective.

(2) By setting up a digital twin system to achieve fault diagnosis and 3D visualization monitoring of PMSM, equipment running status and data can be reflected more visually to quickly locate the PMSM fault and determine the fault type, which shortens the equipment maintenance time and increases the efficiency of coal mining.

Considering the practicality, our current main work is to carry out 3D visual monitoring of belt conveyor and fault diagnosis of its PMSM. However, with the continuous improvement and development of digital twin technology, our future goal is to perform predictive maintenance and full life cycle management of equipment in the coal-mining process, and to apply the proposed theory and method to actual production.

Abbreviations

Abbreviations	English Full Name
PMSM	Permanent Magnet Synchronous Motor
SSA	Sparrow Search Algorithm
ISSA-RF	Improved Sparrow Search Algorithm Optimized Random Forest
RF	Random Forest
BP	Back Propagation
SVM	Support Vector Machine
AC	Alternating Current
VGG	Visual Geometry Group
EMD	Empirical Mode Decomposition
VMD	Variational Mode Decomposition
LSTM	Long Short-Term Memory
WOA	Whale Optimization Algorithm
GWO	Grey Wolf Optimization Algorithm
PSO	Particle Swarm Optimization
MQTT	Message Queuing Telemetry Transport
OPC	OLE for Process Control
OPC UA	OPC Unified Architecture
B_f	Fault Behavior
t_f	Fault Type
d_f	Fault Degree
p_f	Fault Position
m_f	Fault Model
MT_{PMSM}	Permanent Magnet Synchronous Motor Twin Model
G_m	Geometric Model
P_m	Physical Model
R_m	Rule Model,
B_m	Behavior Model

References

1. Hou, C.; Qiao, T.; Zhang, H.; Pang, Y.; Xiong, X. Multispectral visual detection method for conveyor belt longitudinal tear. *Measurement* **2019**, *143*, 246–257. [CrossRef]
2. Feng, Y.; Zhang, M.; Li, G.; Meng, G. Dynamic characteristic analysis and startup optimization design of an intermediate drive belt conveyor with non-uniform load. *Sci. Prog.* **2020**, *103*, 0036850419881089. [CrossRef] [PubMed]
3. Rodriguez, J.; Pontt, J.; Becker, N.; Weinstein, A. Regenerative drives in the megawatt range for high performance downhill belt conveyors. *IEEE Trans. Ind. Appl.* **2002**, *38*, 203–210. [CrossRef]
4. Song, Y.; Zhang, Z.; Yu, S.; Zhang, F.; Zhang, Y. Analysis and reduction of cogging torque in direct-drive external-rotor permanent magnet synchronous motor for belt conveyor application. *IET Electr. Power Appl.* **2021**, *15*, 668–680. [CrossRef]
5. TOrlowska-Kowalska Wolkiewicz, M.; Pietrzak, P.; Skowron, M.; Ewert, P.; Tarchala, G.; Krzysztofiak, M.; TKowalski, C. Fault Diagnosis and Fault-Tolerant Control of PMSM Drives–State of the Art and Future Challenges. *IEEE Access* **2022**, *10*, 59979–60024. [CrossRef]
6. Yang, C.; Bu, L.; Chen, B. Energy modeling and online parameter identification for permanent magnet synchronous motor driven belt conveyors. *Measurement* **2021**, *178*, 109342. [CrossRef]
7. Li, S.; Zhou, X. Sensorless Energy Conservation Control for Permanent Magnet Synchronous Motors Based on a Novel Hybrid Observer Applied in Coal Conveyer Systems. *Energies* **2018**, *11*, 2554. [CrossRef]
8. Lu, E.; Li, W.; Yang, X.; Xu, S. Composite Sliding Mode Control of a Permanent Magnet Direct-Driven System for a Mining Scraper Conveyor. *IEEE Access* **2017**, *5*, 22399–22408. [CrossRef]
9. MA, S.H. Study on the application of permanent magnet synchronous motors in underground belt conveyors. *IOP Conf. Ser. Mater. Sci. Eng.* **2017**, *283*, 012006. [CrossRef]
10. Feng, G.H.; Yu, J.Y.; Zhang, B.Y.; Wang, B.; Sun, H. Study on belt conveyor direct driven by external-rotor PMSM. *Adv. Mater. Res.* **2013**, *619*, 14–17. [CrossRef]
11. Leboeuf, N.; Boileau, T.; Nahid-Mobarakeh, B.; Clerc, G.; Meibody-Tabar, F. Real-Time Detection of Interturn Faults in PM Drives Using Back-EMF Estimation and Residual Analysis. *IEEE Trans. Ind. Appl.* **2011**, *47*, 2402–2412. [CrossRef]
12. Faiz, J.; Nejadi-Koti, H.; Exiri, A.H. Inductance-based inter-turn fault detection in permanent magnet synchronous machine using magnetic equivalent circuit model. *Electr. Power Compon. Syst.* **2017**, *45*, 1016–1030. [CrossRef]

13. Aubert, B.; Régnier, J.; Caux, S.; Alejo, D. Kalman-Filter-Based Indicator for Online Interturn Short Circuits Detection in Permanent-Magnet Synchronous Generators. *IEEE Trans. Ind. Electron.* **2015**, *62*, 1921–1930. [CrossRef]

14. Jokic, S.; Cincar, N.; Novakovic, B. The analysis of vibration measurement and current signature in motor drive faults detection. In Proceedings of the 2018 17th International Symposium INFOTEH-JAHORINA (INFOTEH), East Sarajevo, Bosnia and Herzegovina, 21–23 March 2018; pp. 1–6. [CrossRef]

15. Elbouchikhi, E.; Choqueuse, V.; Auger, F.; Benbouzid, M.E.H. Motor Current Signal Analysis Based on a Matched Subspace Detector. *IEEE Trans. Instrum. Meas.* **2017**, *66*, 3260–3270. [CrossRef]

16. Heydarzadeh, M.; Zafarani, M.; Nourani, M.; Akin, B. A wavelet-based fault diagnosis approach for permanent magnet synchronous motors. *IEEE Trans. Energy Convers.* **2018**, *34*, 761–772. [CrossRef]

17. Li, Y.; Wang, Y.; Zhang, Y.; Zhang, J. Diagnosis of Inter-turn Short Circuit of Permanent Magnet Synchronous Motor Based on Deep learning and Small Fault Samples. *Neurocomputing* **2021**, *442*, 348–358. [CrossRef]

18. Wang, C.S.; Kao, I.H.; Perng, J.W. Fault diagnosis and fault frequency determination of permanent magnet synchronous motor based on deep learning. *Sensors* **2021**, *21*, 3608. [CrossRef]

19. Haddad, R.Z.; Strangas, E.G. On the Accuracy of Fault Detection and Separation in Permanent Magnet Synchronous Machines Using MCSA/MVSA and LDA. *IEEE Trans. Energy Convers.* **2016**, *31*, 924–934. [CrossRef]

20. Arellano-Padilla, J.; Sumner, M.; Gerada, C. Winding condition monitoring scheme for a permanent magnet machine using high-frequency injection. *IET Electr. Power Appl.* **2011**, *5*, 89–99. [CrossRef]

21. Alameh, K.; Cité, N.; Hoblos, G.; Barakat, G. Feature extraction for vibration-based fault detection in Permanent Magnet Synchronous Motors. In Proceedings of the 2015 Third International Conference on Technological Advances in Electrical, Electronics and Computer Engineering (TAEECE), Beirut, Lebanon, 29 April –1 May 2015; pp. 163–168. [CrossRef]

22. Alvarez-Gonzalez, F.; Griffo, A.; Wang, B. Permanent magnet synchronous machine stator windings fault detection by Hilbert–Huang transform. *J. Eng.* **2019**, *2019*, 3505–3509. [CrossRef]

23. Ullah, Z.; Lodhi, B.A.; Hur, J. Detection and Identification of Demagnetization and Bearing Faults in PMSM Using Transfer Learning-Based VGG. *Energies* **2020**, *13*, 3834. [CrossRef]

24. DOĞAN, Z.; SELÇUK, R. A Diagnosis of Stator Winding Fault Based on Empirical Mode Decomposition in PMSMs. *Balk. J. Electr. Comput. Eng.* **2020**, *8*, 73–80.

25. Zhang, K.; Kang, L.; Chen, X.; He, M.; Zhu, C.; Li, D. A Review of Intelligent Unmanned Mining Current Situation and Development Trend. *Energies* **2022**, *15*, 513. [CrossRef]

26. Tao, F.; Zhang, M. Digital Twin Shop-Floor: A New Shop-Floor Paradigm Towards Smart Manufacturing. *IEEE Access* **2017**, *5*, 20418–20427. [CrossRef]

27. Qi, Q.; Tao, F. Digital Twin and Big Data Towards Smart Manufacturing and Industry 4.0: 360 Degree Comparison. *IEEE Access* **2018**, *6*, 3585–3593. [CrossRef]

28. Qi, Q.; Tao, F.; Hu, T.; Anwer, N.; Liu, A.; Wei, Y.; Wang, L.; Nee, A.Y.C. Enabling technologies and tools for digital twin. *J. Manuf. Syst.* **2021**, *58*, 3–21. [CrossRef]

29. Kazała, R.; Luściński, S.; Strączyński, P.; Taneva, A. An Enabling Open-Source Technology for Development and Prototyping of Production Systems by Applying Digital Twinning. *Processes* **2022**, *10*, 21. [CrossRef]

30. Liu, S.; Bao, J.; Lu, Y.; Li, J.; Lu, S.; Sun, X. Digital twin modeling method based on biomimicry for machining aerospace compo-nents. *J. Manuf. Syst.* **2021**, *58*, 180–195. [CrossRef]

31. Wang, K.; Hu, Q.; Liu, J. Digital Twin-Driven Approach for Process Management and Traceability towards Ship Industry. *Processes* **2022**, *10*, 1083. [CrossRef]

32. Lu, Y.; Liu, C.; Kevin, I.; Wang, K.; Huang, H.; Xu, X. Digital Twin-driven smart manufacturing: Connotation, reference model, appli-cations and research issues. *Robot. Comput. -Integr. Manuf.* **2020**, *61*, 101837. [CrossRef]

33. Nejad, R.M.; Rizi, P.N.; Zoei, M.S.; Aliakbari, K.; Ghasemi, H. Failure Analysis of a Working Roll Under the Influence of the Stress Field Due to Hot Rolling Process. *J. Fail. Anal. Prev.* **2021**, *21*, 870–879. [CrossRef]

34. Aliakbari, K.; Nejad, R.M.; Mamaghani, T.A.; Pouryamout, P.; Asiabaraki, H.R. Failure analysis of ductile iron crankshaft in compact pickup truck diesel engine[C]//Structures. *Elsevier* **2022**, *36*, 482–492.

35. Liu, X.; Jiang, D.; Tao, B.; Jiang, G.; Sun, Y.; Kong, J.; Tong, X.; Zhao, G.; Chen, B. Genetic Algorithm-Based Trajectory Optimization for Digital Twin Robots. *Front. Bioeng. Biotechnol.* **2022**, *9*, 793782. [CrossRef] [PubMed]

36. Tao, F.; Zhang, M.; Liu, Y.; Nee, A.Y.C. Digital twin driven prognostics and health management for complex equipment. *Cirp Ann.* **2018**, *67*, 169–172. [CrossRef]

37. Tao, F.; Qi, Q. New IT driven service-oriented smart manufacturing: Framework and characteristics. *IEEE Trans Syst. Man. Cybern Syst.* **2019**, *49*, 81–91. [CrossRef]

38. Da Silva Mendonça, R.; de Oliveira Lins, S.; de Bessa, I.V.; de Carvalho Ayres, F.A.J.; de Medeiros, R.L.P.; de Lucena, V.F.J. Digital Twin Applications: A Survey of Recent Advances and Challenges. *Processes* **2022**, *10*, 744. [CrossRef]

39. Yan, X.; Duan, G. The Real-Time Prediction of Product Quality Based on the Equipment Parameters in a Smart Factory. *Processes* **2022**, *10*, 967. [CrossRef]

40. Wan, Z.; Dong, Y.; Yu, Z.; Lv, H.; Lv, Z. Semi-supervised support vector machine for digital twins based brain image fusion. *Front. Neurosci.* **2021**, *15*, 705323. [CrossRef]

41. Maanani, Y.; Menacer, A. Modeling and Diagnosis of the Inter-Turn Short Circuit Fault for the Sensorless Input-Output Linearization Control of the PMSM. *Period. Polytech. Electr. Eng. Comput. Sci.* **2019**, *63*, 159–168. [CrossRef]
42. Breiman, L. Random forests. *Mach. Learn.* **2001**, *45*, 5–32. [CrossRef]
43. Guo, K.; Wan, X.; Liu, L.; Liu, L.; Gao, Z.; Yang, M. Fault diagnosis of intelligent production line based on digital twin and improved random forest. *Appl. Sci.* **2021**, *11*, 7733. [CrossRef]
44. Xue, J.; Shen, B. A novel swarm intelligence optimization approach: Sparrow search algorithm. *Syst. Sci. Control. Eng.* **2020**, *8*, 22–34. [CrossRef]
45. Jianhua, L.; Zhiheng, W. A hybrid sparrow search algorithm based on constructing similarity. *IEEE Access* **2021**, *9*, 117581–117595. [CrossRef]
46. Ling, G.; Wang, Z.; Shi, Y.; Wang, J.; Lu, Y.; Li, L. Membrane Fouling Prediction Based on Tent-SSA-BP. *Membranes* **2022**, *12*, 691. [CrossRef] [PubMed]
47. Chen, S.; Wang, S. An optimization method for an integrated energy system scheduling process based on NSGA-II improved by tent mapping chaotic algorithms. *Processes* **2020**, *8*, 426. [CrossRef]
48. Tang, Y.; Li, C.; Li, S.; Cao, B.; Chen, C. A fusion crossover mutation sparrow search algorithm. *Math. Probl. Eng.* **2021**, *2021*, 9952606. [CrossRef]
49. Xiong, J.; Liang, W.; Liang, X.; Yao, J. Intelligent quantification of natural gas pipeline defects using improved sparrow search algorithm and deep extreme learning machine. *Chem. Eng. Res. Des.* **2022**, *183*, 567–579. [CrossRef]
50. Kassaymeh, S.; Al-Laham, M.; Al-Betar, M.A.; Alweshah, M.; Abdullah, S.; Makhadmeh, S. Backpropagation Neural Network optimization and software defect estimation modelling using a hybrid Salp Swarm optimizer-based Simulated Annealing Algorithm. *Knowl.-Based Syst.* **2022**, *244*, 108511. [CrossRef]
51. Liu, C.; Vengayil, H.; Lu, Y.; Xu, X. A cyber-physical machine tools platform using OPC UA and MTConnect. *J. Manuf. Syst.* **2019**, *51*, 61–74. [CrossRef]